J Mater Sci: Mater Med (2009) 20:1347–1355
DOI 10.1007/s10856-009-3698-0

Aspects of the in vitro bioactivity and antimicrobial properties of Ag^+- and Zn^{2+}-exchanged 11 Å tobermorites

Nichola J. Coleman

Received: 18 November 2008 / Accepted: 22 January 2009 / Published online: 13 February 2009

Abstract 11 Å tobermorite, $Ca_5Si_6O_{16}(OH)_2 \cdot 4H_2O$, is a layer lattice ion exchange mineral whose potential as a carrier for Ag^+ and Zn^{2+} ions in antimicrobial, bioactive formulations has not yet been explored. In view of this, the in vitro bioactivity of Ag^+- and Zn^{2+}-exchanged 11 Å tobermorites and their bactericidal action against *S. aureus* and *P. aeruginosa* are reported. The in vitro bioactivity of the synthetic unsubstituted tobermorite phase was confirmed by the formation of bone-like hydroxycarbonate apatite (HCA) on its surface within 48 h of contact with simulated body fluid. The substitution of labile Ag^+ ions into the tobermorite lattice delayed the onset of HCA-formation to 72 h; whereas, the Zn^{2+}-substituted phase failed to elicit an HCA-layer within 14 days. Both Ag^+- and Zn^{2+}-exchanged tobermorite phases were found to exhibit marked antimicrobial action against *S. aureus* and *P. aeruginosa*, two common pathogens in biomaterial-centred infections.

1 Introduction

11 Å tobermorite, $Ca_5Si_6O_{16}(OH)_2 \cdot 4H_2O$, is a rare naturally-occurring layer-lattice ion exchange mineral which is also readily synthesised from a variety of reagents under alkaline hydrothermal conditions between 80 and 200°C [1–4]. Its ideal structure comprises infinite double layers of Ca–O polyhedra linked on both sides to wollastonite-like silicate chains running along the *b*-axis, as shown in Fig. 1. This assembly is stacked in the *c*-direction creating interlayer channels which accommodate water molecules and labile cations (usually Ca^{2+} and/or Na^+ ions).

It is now widely acknowledged that certain bioactive glass, ceramic and mineral phases can integrate with living bone tissue in vivo [5, 6]. This material-cell interface usually develops via the spontaneous precipitation of a layer of substituted hydroxycarbonate apatite (HCA), $(Ca,Mg,Na)_{10}(PO_4,CO_3)_6(OH)_2$, from ions present in human plasma. The resulting superficial HCA layer is similar in structure to the mineral component of bone and provides a focus for the attachment and proliferation of new bone-forming cells. These bioactive materials are used to repair diseased or damaged bone tissue and can be designed to remain in situ indefinitely or to degrade as the normal functions of the host tissue are restored. Lin and coworkers have recently demonstrated that tobermorite nanofibres exhibit the property of bioactivity and their initial in vitro study indicates that the tobermorite lattice is likely to degrade in the physiological environment [7].

The occurrence of biomaterial-centred sepsis restricts the scope and success of bioactive implants and accordingly problems presented by postoperative infection following implantation have stimulated research into the development of bioactive materials with concomitant antimicrobial properties [8–11]. During the past decade, silver nanoparticles, salts and complexes have been incorporated into bioactive materials, pharmaceutical formulations and biomedical devices to exploit the broad-spectrum antimicrobial characteristics of the Ag^+ ion [12–14]. The precise mechanisms by which silver exerts its toxicity are not yet fully defined, although it is acknowledged that Ag^+ ions inhibit bacterial enzymes, bind to DNA and interfere with electron transport processes.

N. J. Coleman (✉)
School of Science, University of Greenwich, Chatham Maritime, Kent ME4 4TB, UK
e-mail: nj_coleman@yahoo.co.uk

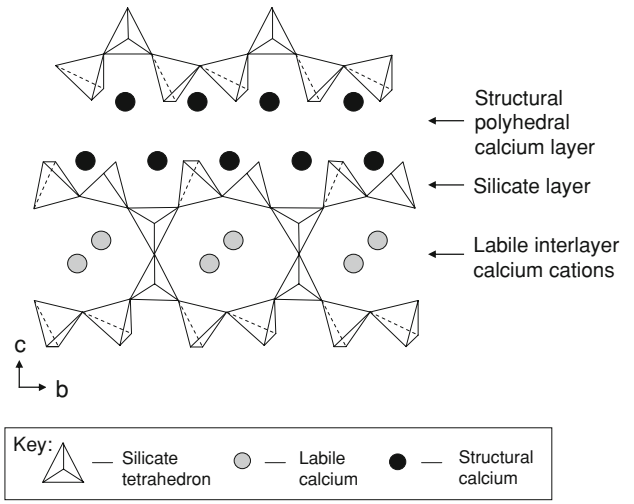

Fig. 1 Projection of 11 Å tobermorite in the *bc*-plane

Zinc is an essential antioxidant and anti-inflammatory agent in the human body, deficiency in which causes delayed wound healing, immune dysfunction, growth retardation and neuro-sensory disorders. In the human body Zn^{2+} ions are associated with the structure and function of a large number of macromolecules and are essential to over 300 enzymic processes which include the regulation of bone growth and the replication of DNA. Zinc inhibits nutrient uptake in bacteria and interferes with proton transfer processes; its antimicrobial action is less extensive than that of silver although its wound healing and bactericidal properties are similarly exploited in a range of healthcare products [14, 15].

In the present study, the in vitro bioactivity and antibacterial action of Ag^{+}- and Zn^{2+}-exchanged 11 Å tobermorites (Tob-Ag and Tob-Zn, respectively) are evaluated relative to those of the as-synthesised Na^{+}-bearing phase (Tob-Na). *Staphylococcus aureus* (gram-positive) and *Pseudomonas aeruginosa* (gram-negative) were selected for this investigation as they are known to cause biomaterial-centred infections and resistant septic conditions in tissues such as bones, teeth and skin [9].

2 Materials and methods

2.1 Preparation of 11 Å tobermorites, Tob-Na, Tob-Ag and Tob-Zn

11 Å tobermorite specimens, Tob-Na, were prepared in duplicate by heating 6.8 g of $Na_2SiO_3 \cdot 5H_2O$, 1.47 g of CaO and 60 cm^3 of 1 M $NaOH_{(aq)}$ at 100°C in sessile hermetically-sealed PTFE reaction vessels under autogenous pressure for 19 days. The products of each synthesis were washed with deionised water to pH ~7, dried to constant mass in air at 40°C and stored in air-tight polypropylene containers until required. Analysis of the reaction products by powder X-ray diffraction (XRD), X-ray fluorescence spectroscopy (XRF) and scanning electron microscopy (SEM) is described elsewhere [16].

Ag^{+}- and Zn^{2+}-exchanged tobermorite specimens, Tob-Ag and Tob-Zn, were prepared in triplicate from Tob-Na specimens by ion exchange under sessile batch conditions using single metal nitrate solutions at 25°C. In each case 0.5 g of Tob-Na was added to 200 cm^3 of either 3.0 mM $AgNO_{3(aq)}$ or 5.0 mM $Zn(NO_3)_{2(aq)}$ in a screw-capped polypropylene bottle. The supernatant metal ion concentrations were monitored by inductively coupled plasma analysis (ICP) at intervals between 15 minutes and 9 days, after which time the ion-exchanged solids were separated by gravitational filtration, washed with deionised water, dried to constant mass in air at 40°C and analysed by XRF. Oxide compositions and formulae for samples Tob-Na, Tob-Ag and Tob-Zn were derived from XRF analysis are listed in Table 1.

2.2 In vitro bioactivity of Tob-Na, Tob-Ag and Tob-Zn

Simulated body fluid (SBF) was prepared in accordance with the method described by Kokubo and Takadama [6] and stored at 4°C for no longer than 3 days prior to use. 0.04 g of either Tob-Na, Tob-Ag or Tob-Zn were contacted with 40 cm^3 of SBF in hermetically sealed polypropylene containers at 37°C for time intervals of 3, 6, 24, 48, 72 and 168 h. Each analysis was carried out in

Table 1 Oxide compositions and formulae of tobermorite specimens Tob-Na, Tob-Ag and Tob-Zn

Sample	Oxide composition (mass %)						Formula
	SiO_2	CaO	Na_2O	Ag_2O	ZnO	H_2O[a]	
Tob-Na	48.40	34.25	1.83	–	–	15.46	$Ca_{4.55}Na_{0.44}Si_{6.00}O_{16.77} \cdot 6.4\ H_2O$
Tob-Ag	39.58	24.99	0.14	11.71	–	23.55	$Ca_{4.06}Na_{0.04}Ag_{0.92}Si_{6.00}O_{16.54} \cdot 11.9\ H_2O$
Tob-Zn	44.99	22.32	0.27	–	20.24	12.14	$Ca_{3.19}Na_{0.07}Zn_{1.99}Si_{6.00}O_{17.21} \cdot 5.4\ H_2O$

[a] Calculated from loss-on-ignition at 1000°C

triplicate. The pH values of the supernatant liquors were measured using a Corning 140 pH meter and solution concentrations of Si, Ca, P, Ag and Zn species were monitored by ICP using a TJA Iris simultaneous ICP-OES and matrix-matched multi-element standards. The solid specimens were recovered by filtration, washed once with distilled water and dried in air at 37°C for 24 h prior to analysis by Fourier transform infrared spectroscopy (FTIR) using a Perkin Elmer Paragon 1000 FTIR spectrophotometer. Spectra were recorded between 4000 and 500 cm^{-1} using KBr discs.

The dissolution ratio (S) of the tobermorite specimens in SBF was calculated according to the following relationship (after Lin et al. [7]):

$$S = \frac{(c_{Si} \times v)}{m_{Si}} \times 100\%$$

where c_{Si}, v and m_{Si} are the Si concentration in SBF (mg cm^{-3}), volume of SBF (cm^3) and initial silicon-content of the tobermorite samples (mg), respectively (i.e. S is the percentage of the silicate lattice which has undergone dissolution).

2.3 Antibacterial evaluation of Tob-Na, Tob-Ag and Tob-Zn

Samples Tob-Na, Tob-Ag or Tob-Zn at concentrations of 10.0 mg cm^{-3} were added in triplicate to separate McCartney bottles containing 10 cm^3 of Nutrient Broth (Oxoid). These tubes were inoculated with cultures of *Staphylococcus aureus* NCIMB 9518 or *Pseudomonas aeruginosa* NCIMB 8628 to densities of 4.1×10^4 and 5.6×10^6 colony forming units per cm^3 (CFU cm^{-3}), respectively. The cultures were then incubated, with shaking, at 37°C overnight and duplicate plate counts on Nutrient Both (Oxoid) were taken for each assay. Cultures with no added tobermorite were also analysed as controls.

Viable cell count data for the cultures containing tobermorite samples were compared with those of the control culture populations. In each case, the null hypothesis that the two measurements are not significantly different was tested at the 95% significance level using a one-tailed *t*-test. The observed value of t was estimated as:

$$t = \frac{\bar{x}_d \sqrt{n}}{S_d}$$

where n is the number of data pairs, $\bar{x}_d$ is the mean of the differences between the data pairs and S_d is the standard deviation of $\bar{x}_d$. If the tabulated critical t value was found to be greater than the observed (calculated) value of $|t|$, the null hypothesis was retained.

3 Results

3.1 Characterisation and ion exchange properties of Tob-Na

The powder XRD pattern of specimen Tob-Na (Fig. 2a) is similar to those of other synthetic phase-pure crystalline 11 Å tobermorites reported in the literature [17, 18]. Traces of calcite, $CaCO_3$, are also present and commonly arise from atmospheric carbonation during the hydrothermal preparation of tobermorites. Scanning electron microscopy revealed that Tob-Na comprises irregularly shaped particles, typically between 20 and 40 μm in diameter (Fig. 2b), whose surfaces are populated by a network of platy foils which are characteristic of the morphology of tobermorite [16, 19].

The uptake profile for Ag^+ by Tob-Na is plotted in Fig. 3 and shows that equilibrium is achieved within 24 h, by which time the extent of Ag^+-uptake is 10.4 wt% (0.96 mmol g^{-1}). XRF analysis of the Ag^+-exchanged tobermorite phase, Tob-Ag, indicated that 91% and 10.8% of the original Na^+ and Ca^{2+} ions had, respectively, been exchanged for incoming Ag^+ ions (Table 1). These data suggest that the majority of labile interlayer Na^+ and Ca^{2+} ions is readily exchanged for Ag^+ ions, and that the remaining four Ca^{2+} ions per unit formula which constitute the structural Ca–O

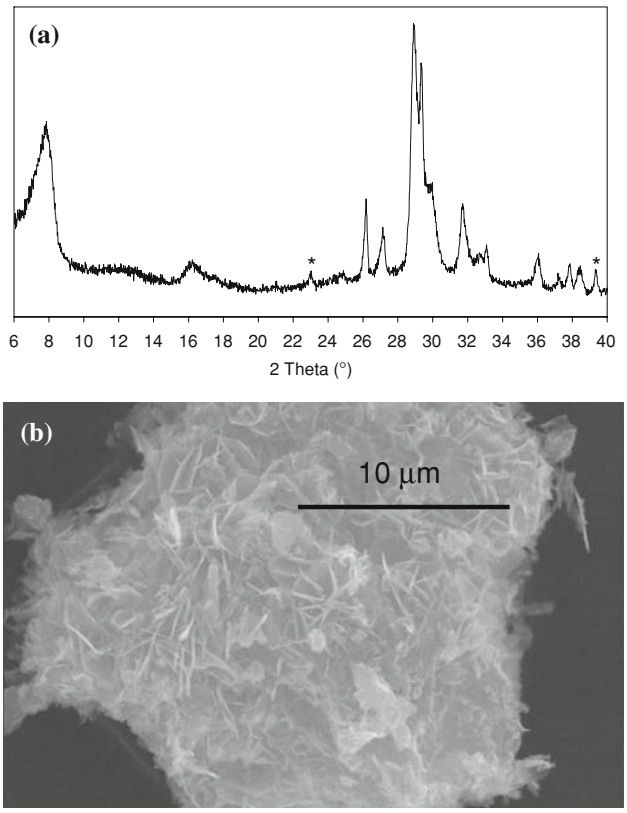

Fig. 2 **a** Powder XRD patterns of Tob-Na (asterisks denote reflections from calcite) and **b** SEM micrograph of Tob-Na particle

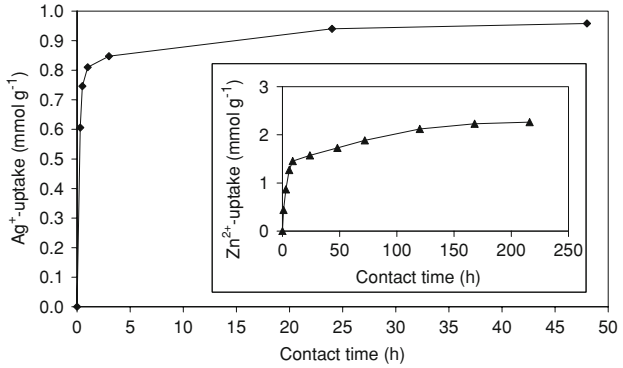

Fig. 3 Uptake profiles of Ag^{+} and Zn^{2+} (inset) by Tob-Na

polyhedral layer are not available for reaction with Ag^{+} under the selected conditions.

The uptake profile for Zn^{2+} ions by Tob-Na is inset in Fig. 3 and shows that a steady state is not established within the 216 h observation period, by which time Zn^{2+}-uptake is found to be 12.4 wt% (2.26 mmol g^{-1}). XRF analysis demonstrated that, in addition to the exchange of labile cations, approximately 20% of the 'structural' Ca^{2+} ions from the polyhedral layer also participate in the Zn^{2+}-exchange process.

The formulae of Tob-Na, Tob-Ag and Tob-Zn are listed in Table 1 and their FTIR spectra are shown in Figs. 4a, 5a and 6a, respectively. In each spectrum, the combination band at $\sim$960 cm^{-1} arises from various Si–O stretching modes and the sharp signal at 680 cm^{-1} is attributed to Si–O–Si bending vibrations [20, 21]. The bands at 1460 and 867 cm^{-1} derive from carbonate ion stretching and bending modes, respectively, and the broad signals at 1630 and 3450 cm^{-1} arise from O–H vibrations of interlayer water molecules and silanol species. Weak, broad bands at $\sim$790 cm^{-1} arising from bending vibrations in amorphous silica are also present in the spectra of Tob-Ag and Tob-Zn and indicate that some amorphisation of the tobermorite lattice took place during the ion exchange reactions.

3.2 In vitro bioactivity of Tob-Na, Tob-Ag and Tob-Zn

The FTIR spectra of Tob-Na following in vitro exposure to SBF for up to 168 h are shown in Fig. 4 and the corresponding supernatant concentrations of calcium, silicate and phosphate species are presented in Fig. 7. A weak,

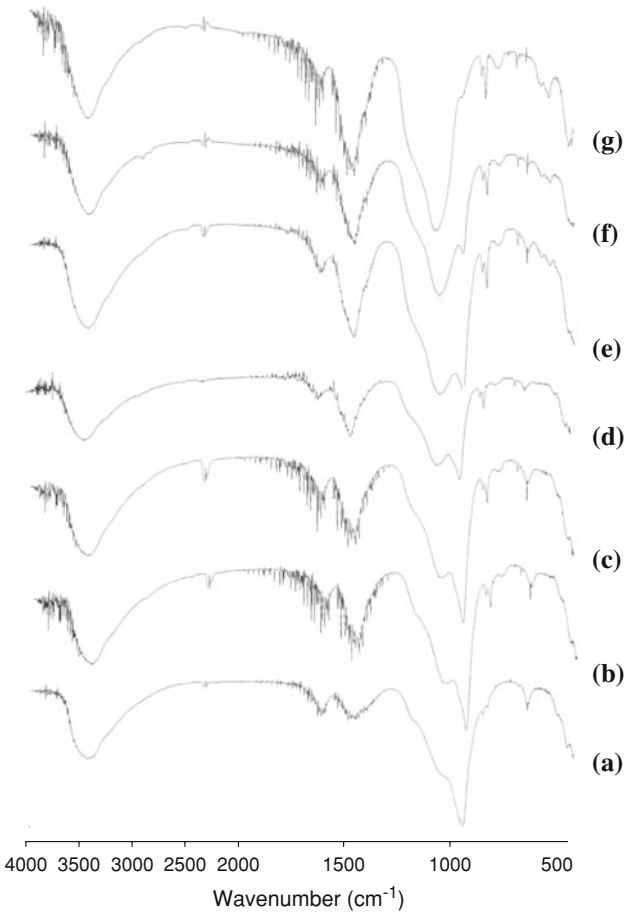

Fig. 4 FTIR spectra of Tob-Na following immersion in SBF for (a) 0 h; (b) 3 h; (c) 6 h; (d) 24 h; (e) 48 h; (f) 72 h and (g) 168 h

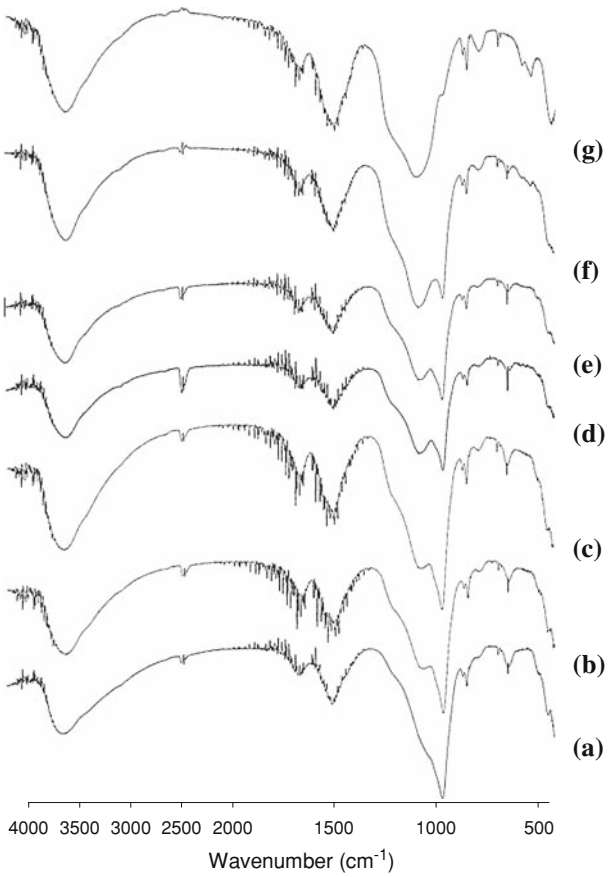

Fig. 5 FTIR spectra of Tob-Ag following immersion in SBF for (a) 0 h; (b) 3 h; (c) 6 h; (d) 24 h; (e) 48 h; (f) 72 h and (g) 168 h

broad signal at ~790 cm^{-1} appears in the FTIR spectrum of Tob-Na within 3 h of contact with SBF (Fig. 4b) which denotes the presence of amorphous silica and indicates that the tobermorite lattice has begun to degrade. The silicate solution profile data (Fig. 7c) is consistent with this observation and shows that within 3 h the concentration of silicate ions in SBF rises from zero to 32.5 ppm which corresponds with the dissolution of ~17% of the silicate species from the original Tob-Na lattice. The concomitant increase in calcium ion concentration (Fig. 7b) and rise in SBF solution pH (Fig. 8a) are also indicative of the dissolution of the tobermorite lattice.

By 48 h, the intensities of the carbonate ion bands at 867 and 1460 cm^{-1} in the FTIR spectrum of Tob-Na increase and the combination Si–O band at ~960 cm^{-1} is partially obscured by the development of a broad P–O stretching signal at 1070 cm^{-1} (Fig. 4e). These observations and the concurrent appearance of a doublet arising from P–O bending vibrations at 560 and 590 cm^{-1} confirm the deposition of crystalline HCA on the surface of Tob-Na within 48 h of exposure to SBF [22].

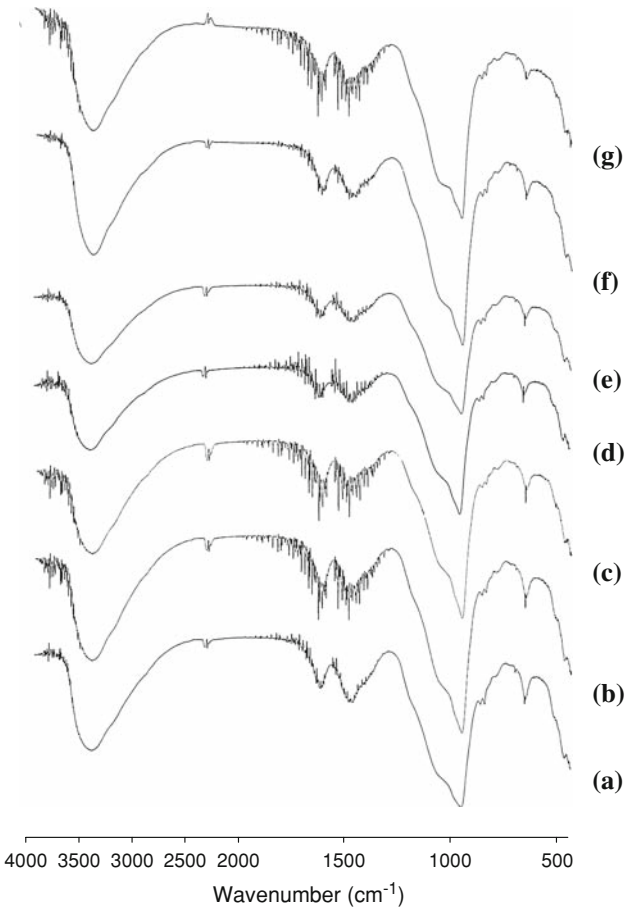

Fig. 6 FTIR spectra of Tob-Zn following immersion in SBF for (a) 0 h; (b) 3 h; (c) 6 h; (d) 24 h; (e) 48 h; (f) 72 h and (g) 168 h

FTIR spectra of Tob-Ag as functions of residence time in SBF are presented in Fig. 5. Evidence for the formation of crystalline HCA is denoted by the poorly resolved doublet at 565 and 595 cm^{-1} after 72 h, whose intensity and resolution are markedly increased by 168 h (Fig. 5f, g, respectively). The concomitant removal of phosphate species from SBF and dissolution of calcium and silicate components from the tobermorite lattice are shown in Fig. 7. The silver-release profile for Tob-Ag is presented in Fig. 8b and shows that the maximum silver concentration of SBF does not exceed 0.15 ppm (i.e. 0.14% of the total Ag^{+}-content) throughout the duration of the investigation.

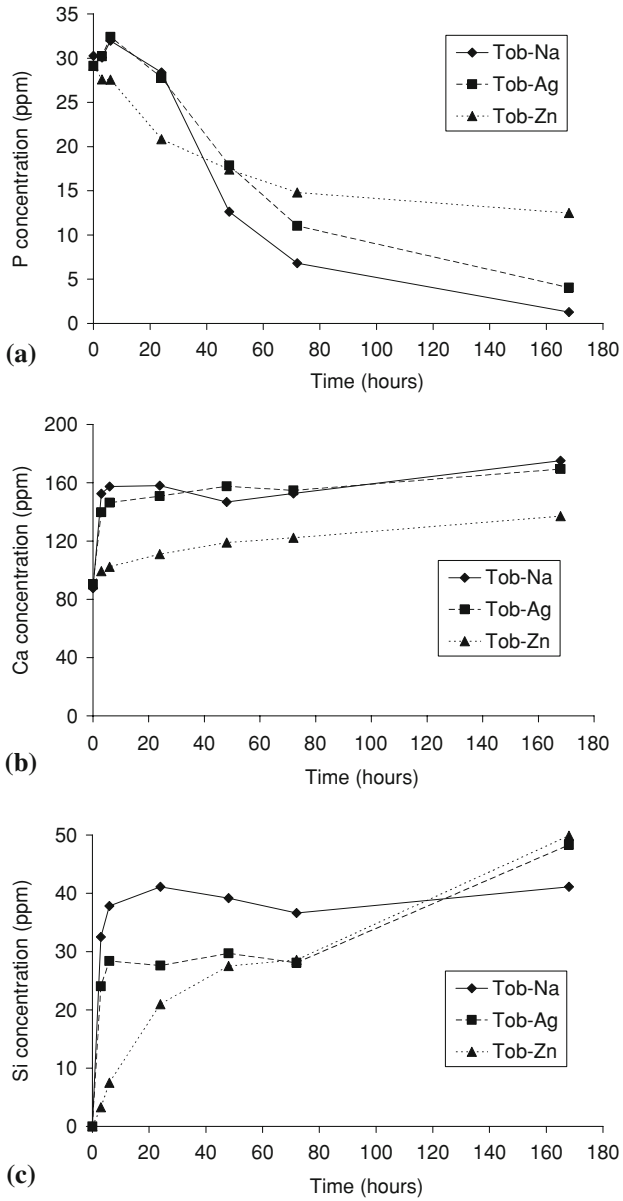

Fig. 7 Concentrations of **a** phosphorous; **b** calcium and **c** silicon as functions of residence time in SBF

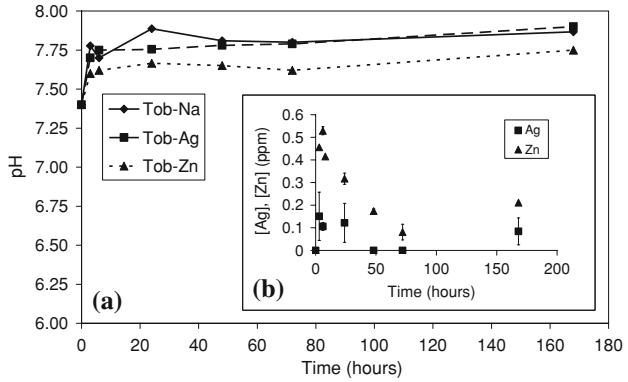

Fig. 8 **a** Solution pH profiles and **b** concentrations of silver and zinc (inset) as functions of residence time in SBF

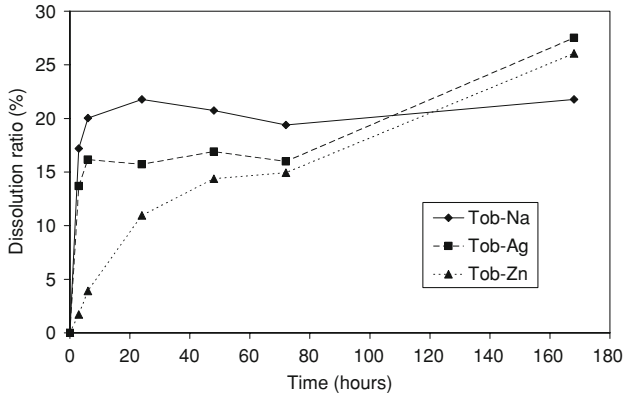

Fig. 9 Dissolution ratios of Tob-Na, Tob-Ag and Tob-Zn as functions of residence time in SBF

FTIR spectra of Tob-Zn following exposure to SBF for up to 168 h are shown in Fig. 6 and indicate that this material does not elicit the nucleation and growth of HCA within this timeframe. On the basis of this finding, additional Tob-Zn specimens were exposed to SBF solutions for 14 days, and similarly, no evidence for HCA-formation was detected during this extended observation period. In spite of the absence of superficial HCA, the initial rate of phosphate removal from SBF by Tob-Zn is greater than those of Tob-Na and Tob-Ag (Fig. 7a) and the phosphate concentration of SBF in contact with Tob-Zn falls to 12.5 ppm within 168 h. The fate of the phosphate ions is presently unknown, although they are likely to be adsorbed to the surface of Tob-Zn in some form other than HCA. In this case, characteristic P–O stretching modes would be anticipated in the approximate range 1000–1100 cm^{-1}, and may indeed be present yet concealed by the strong combination Si–O stretching bands in this region.

Analysis of the supernatant SBF solutions in contact with Tob-Zn indicates that the release of calcium ions from the lattice (Fig. 7b) and accompanying rise in pH (Fig. 8a) are less extensive than those observed for specimens Tob-Ag and Tob-Zn. The zinc release profile is presented in Fig. 8b and shows that the maximum zinc concentration of SBF, 0.53 ppm, occurs after 6 h and corresponds with the dissolution of 0.43% of the original Zn^{2+}-content of Tob-Zn.

The dissolution ratios for Tob-Na, Tob-Ag and Tob-Zn are plotted in Fig. 9 as functions of residence time in SBF. The dissolution ratio profile for Tob-Na is similar to that reported by Lin et al. [7] for synthetic unsubstituted tobermorite. In comparison, the initial rate of degradation of the Ag- and Zn-substituted tobermorites is slower than that of their unsubstituted counterpart, although ultimately this trend is reversed.

3.3 Antibacterial properties of Tob-Na, Tob-Ag and Tob-Zn

The results of the in vitro antibacterial assays are listed in Table 2 and indicate that the original tobermorite specimen, Tob-Na, exhibits a modest inhibitory effect against *P. aeruginosa* at a concentration of 10.0 mg cm^{-3}. Conversely, there was no statistical difference between viable cell counts for *S. aureus* containing 10.0 mg cm^{-3} of Tob-Na and those of the control populations (in a one-tailed *t*-test at $P = 0.05$). In contrast, marked inhibitory effects of greater than five orders of magnitude were noted for Tob-Ag and Tob-Zn

Table 2 Cell count data for control cultures and cultures containing Tob-Na, Tob-Ag and Tob-Zn

	Control	Tob-Na	Tob-Ag	Tob-Zn
S. aureus				
Mean (CFU cm^{-3})	4.7×10^9	3.6×10^9	No count (10^4)	No count (10^4)
St. Dev. (CFU cm^{-3})	3.0×10^9	2.0×10^9	–	–
Observed |t|[a]	–	1.02	–	–
P. aeruginosa				
Mean (CFU cm^{-3})	9.3×10^{10}	4.8×10^9	No count (10^4)	No count (10^4)
SD (CFU cm^{-3})	2.2×10^{10}	1.9×10^9	–	–
Observed |t|[a]	–	4.55	–	–

[a] Critical |t| at ($P = 0.10$) for (n − 1) degrees of freedom is 2.02

against both gram negative *P. aeruginosa* and gram positive *S. aureus*.

4 Discussion

An indication of bioactivity can be obtained by the rate of formation of an hydroxycarbonate apatite layer on the surface of a substrate in simulated body fluid in vitro [6]. Accordingly, this research confirms the findings of Lin et al. [7], that tobermorite exhibits in vitro bioactivity and that the tobermorite lattice degrades on contact with SBF. Recent research has shown that dissolved silicate species from bioactive substrates operate at a genetic level to influence the osteoblast cycle [23, 24]. Soluble silicate species are now known to enhance the expression of genes and increase the production of cytokines and proteins which regulate bone-growth. In this respect, it is envisaged that the release of silicates, as shown in Figs. 7c and 9, will confer additional in vivo bioactivity on tobermorite.

Lin et al. [7] report that the dissolution ratio of tobermorite nanofibres (i.e. the percentage of silicate species which is released into solution via the degradation of the original tobermorite lattice) reached approximately 17.4 and 19.6% within 72 and 168 h, respectively. For comparison, the dissolution ratio of the 20–40 μm diameter tobermorite particles investigated in the present study is plotted as a function of time in Fig. 9 and indicates that the dissolution rates of both particulate Tob-Na and Lin's tobermorite nanofibres are similar irrespective of the marked difference in geometrical surface area between the two specimens. The similarity in the dissolution ratio profiles between the two systems suggests that it is the internal surface area of the layered tobermorite lattice rather than its external geometrical surface area which dictates the dissolution kinetics of this mineral phase.

Labile, interlayer Na^+ and Ca^{2+} ions in Tob-Na were readily exchanged for Ag^+ ions under batch conditions at 25°C; and Zn^{2+} ions were found to replace both interlayer cations and Ca^{2+} ions from the structural polyhedral Ca–O layer. Equilibrium Ag^+-uptake of 0.96 mmol g^{-1} was achieved within 24 h; whereas a steady state for Zn^{2+}-uptake was not established within 218 h, by which time 2.26 mmol g^{-1} of Zn^{2+} ions had been exchanged. In the latter case the superior sorption capacity and slow reaction rate were attributed to the bond-breaking processes and structural rearrangement of the tobermorite lattice which take place during Zn^{2+}-exchange for Ca^{2+} ions from the polyhedral Ca–O layer. These findings are consistent with those of other researchers who report that monovalent cations are rapidly exchanged for labile cations in 11 Å tobermorite and that certain divalent cations also undergo slow exchange for structural Ca^{2+} ions [25, 26].

The exchange of labile interlayer Na^+ and Ca^{2+} ions for Ag^+ ions in tobermorite was found to effect an overall reduction in the rate of removal of phosphate ions from SBF and commensurate delay in the detection of crystalline HCA from 48 to 72 h (Figs. 4, 5 and 7a). The incorporation of interlayer Ag^+ ions also reduced the initial silicate dissolution rate relative to that of its unsubstituted counterpart.

During this investigation, the incorporation of 2.26 mmol g^{-1} of Zn^{2+} into tobermorite resulted in its failure to elicit the formation of HCA from SBF within 14 days. This observation is consistent with those of other researchers who report that zinc exerts a pronounced inhibitory effect on the growth of hydroxyapatite [27, 28]. The biochemical role and therapeutic potential of zinc in bioactive glasses and ceramics is not yet fully understood. Its incorporation into bioactive substrates has been reported to improve their bone-bonding ability by stimulating the proliferation and differentiation of bone cells [29, 30]; yet, research also indicates that the release of zinc from bioactive glasses can cause oxidative damage to human osteoblast cells [31]. It is without doubt that the impact of zinc-bearing substrates on a given tissue-type will depend upon the concentration, release kinetics, speciation and bioavailability of the zinc. In view of this, the potential bioactivity and therapeutic effects of Zn^{2+}-exchanged tobermorites cannot be entirely ruled out since lower levels of zinc-substitution may enable the formation of the HCA layer and stimulate bone cell activity. Accordingly, the next phase of this research will include an investigation of osteoblast adhesion, proliferation and differentiation on Na^+-, Ag^+- and Zn^{2+}-exhanged tobermorite phases as functions of the extent of substitution.

Both Ag^+- and Zn^{2+}-bearing tobermorite samples were found to exhibit marked antibacterial effects against single strains of gram-positive *S. aureus* and gram-negative *P. aeruginosa*; two bacteria which are frequently responsible for postoperative orthopaedic infection. Bacteria are highly adapted to colonise surfaces, and hence, the fate of an available biomaterial surface in vivo is the outcome of a contest between bacterial adhesion and host tissue integration [32, 33]. This competition is mediated by the spontaneous adsorption of host proteins on implantation which provide receptor sites for bacterial or tissue adhesion; for example, *S. aureus* possesses discrete binding sites for collagen and fibronectin. Once bacterial adhesion has occurred on an implant surface it is unlikely that the host tissue cells will subsequently be able to displace these colonies and infection usually persists, in spite of antibiotic therapy, until the implant is removed.

One strategy to promote successful tissue integration over bacterial adhesion is to design implant surfaces which possess intrinsic and persistent antimicrobial properties. In this respect, the incorporation of Ag^+ and Zn^{2+} ions into the tobermorite lattice has been shown to confer

outstanding antibacterial activity against two pathogens which are frequently associated with orthopaedic infection. Additionally, the slow release of Ag^{+} and Zn^{2+} in SBF in vitro indicates that these materials may also provide sustained antimicrobial action.

It should be noted that the potential antibacterial properties of Ag^{+}- and Zn^{2+}-exchanged tobermorites are not restricted to biomaterials applications. Silver- and zinc-exchanged zeolites and clays have been used as coatings and in composites to confer antimicrobial properties to Portland cement mortars [34], food packaging [35], ointments [36], stainless steel [14], paper, paints and plastic products [37]. Tobermorites have a number of technical advantages over zeolites and clays in that they can be prepared, not only as finely dispersed powders, but also as nanofibres and large monolithic articles of variable porosity; they are also thermodynamically stable in Portland cement systems, whereas zeolites and clays degrade by pozzolanic reaction.

5 Conclusions

Labile interlayer Na^{+} and Ca^{2+} ions in synthetic 11 Å tobermorite are readily exchanged for Ag^{+} ions from solution under batch conditions at 25°C; whereas, Zn^{2+} ions are exchanged for both labile cations and 'structural' Ca^{2+} ions from the polyhedral Ca–O layer within the tobermorite lattice. The resulting Ag^{+}- and Zn^{2+}-exchanged phases exhibit marked antimicrobial action against *S. aureus* and *P. aeruginosa*.

The in vitro bioactivity of the unsubstituted tobermorite phase was confirmed by the formation of bone-like hydroxycarbonate apatite (HCA) on its surface within 48 h of contact with simulated body fluid. The substitution of labile Ag^{+} ions into the tobermorite lattice was found to delay the onset of HCA-formation to 72 h and the Zn^{2+}-substituted phase failed to elicit an HCA-layer within 14 days.

Acknowledgements The author acknowledges, with gratitude, financial support for this research from the Royal Society of Chemistry and from The Royal Society.

References

1. S.A. Hamid, Z. Kristalogr. **154**, 189 (1981)
2. S. Merlino, E. Bonaccorsi, T. Armbruster, Eur. J. Mineral. **13**, 577 (2001). doi:10.1127/0935-1221/2001/0013-0577
3. S. Komarneni, D.M. Roy, Science **22**, 647 (1983). doi:10.1126/science.221.4611.647
4. N.J. Coleman, Mater. Res. Bull. **40**, 2000 (2005). doi:10.1016/j.materresbull.2005.05.006
5. T. Kokubo, Mater. Sci. Eng. C **25**, 97 (2005). doi:10.1016/j.msec.2005.01.002
6. T. Kokubo, H. Takadama, Biomaterials **27**, 2907 (2006). doi:10.1016/j.biomaterials.2006.01.017
7. K. Lin, J. Chang, R. Cheng, Acta Biomater. **3**, 271 (2007). doi:10.1016/j.actbio.2006.11.003
8. M. Bellantone, N.J. Coleman, L.L. Hench, J. Biomed. Mater. Res. **51**, 484 (2000). doi:10.1002/1097-4636(20000905)51:3<484::AID-JBM24>3.0.CO;2-4
9. M. Bellantone, N.J. Coleman, L.L. Hench, Key Eng. Mater. **192–195**, 597 (2001)
10. W. Chen, Y. Liu, H.S. Courtney, M. Bettenga, C.M. Agrawal, J.D. Bumgardner, J.L. Ong, Biomaterials **27**, 5512 (2006). doi:10.1016/j.biomaterials.2006.07.003
11. I. Ahmed, D. Ready, M. Wilson, J. Knowles, J. Biomed. Mater. Res. A **79**, 618 (2006). doi:10.1002/jbm.a.30808
12. A.B.G. Lansdown, Curr. Probl. Dermatol. **33**, 17 (2006). doi:10.1159/000093928
13. X. Chen, H.J. Schluesener, Toxicol. Lett. **176**, 1 (2008). doi:10.1016/j.toxlet.2007.10.004
14. K.R. Bright, C.P. Gerba, P.A. Rusin, J. Hosp. Infect. **52**, 307 (2002). doi:10.1053/jhin.2002.1317
15. M.C. Bonferoni, G. Cerri, M. de' Gennaro, C. Juliano, C. Caramella, Appl. Clay Sci. **36**, 95 (2007). doi:10.1016/j.clay.2006.04.014
16. N.J. Coleman, D.S. Brassington, Mater. Res. Bull. **38**, 485 (2003). doi:10.1016/S0025-5408(02)01056-5
17. G.L. Kalousek, J. Am. Ceram. Soc. **40**, 74 (1957). doi:10.1111/j.1151-2916.1957.tb12579.x
18. S. Shaw, C.M.B. Henderson, B.U. Komanschek, Chem. Geol. **167**, 141 (2000). doi:10.1016/S0009-2541(99)00206-5
19. N.J. Coleman, D.S. Brassington, A. Raza, A.P. Mendham, Waste Manag. **26**, 260 (2006). doi:10.1016/j.wasman.2005.01.019
20. R.J. Kirkpatrick, J.L. Yarger, P.F. McMillan, P. Yu, X. Cong, Adv. Cement Base. Mater. **5**, 93 (1997). doi:10.1016/S1065-7355(97)00001-1
21. N.Y. Mostafa, A.A. Shaltout, H. Omarb, S.A. Abo-El-Enein, J. Alloy. Compd. doi:10.1016/j.jallcom.2007.11.130
22. C. Ohtsuki, T. Kokubo, T. Yamamuro, J. Non-Cryst. Solid **143**, 84 (1992). doi:10.1016/S0022-3093(05)80556-3
23. N. Patel, S.M. Best, W. Bonfield, I.R. Gibson, K.A. Hing, E. Damien, P.A. Revell, J. Mater. Sci. Mater. Med. **13**, 1199 (2002). doi:10.1023/A:1021114710076
24. I.D. Xynos, A.J. Edgar, L.D.K. Buttery, L.L. Hench, J.M. Polak, J. Biomed. Mater. Res. **55**, 151 (2001). doi:10.1002/1097-4636(200105)55:2<151::AID-JBM1001>3.0.CO;2-D
25. M. Miyake, S. Komarneni, R. Roy, Mater. Res. Bull. **24**, 311 (1989). doi:10.1016/0025-5408(89)90217-1
26. S. Komarneni, R. Roy, D.M. Roy, Cement Concr. Res. **16**, 47 (1986). doi:10.1016/0008-8846(86)90067-0
27. N. Kanzaki, K. Onuma, G. Treboux, S. Tsutsumi, A. Ito, J. Phys. Chem. B **104**, 4189 (2000). doi:10.1021/jp9939726
28. N. Kanzaki, K. Onuma, G. Treboux, S. Tsutsumi, A. Ito, J. Phys. Chem. B **105**, 1991 (2000). doi:10.1021/jp003295b
29. A. Ito, H. Kawamura, M. Otsuka, M. Ikeuchi, H. Ohgushi, K. Ishikawa, K. Onuma, N. Kanzaki, Y. Sogo, N. Ichinose, Mater. Sci. Eng. C **22**, 21 (2002). doi:10.1016/S0928-4931(02)00108-X
30. A. Ito, M. Otsuka, H. Kawamura, M. Ikeuchi, H. Ohgushi, Y. Sogo, N. Ichinose, Curr. Appl. Phys. **5**, 402 (2005). doi:10.1016/j.cap.2004.10.006
31. V. Aina, A. Perardi, L. Bergandi, G. Malavasi, L. Menabue, C. Morterra, D. Ghigo, Chem. Biol. Interact. **167**, 207 (2007). doi:10.1016/j.cbi.2007.03.002
32. A.G. Gristina, Science **237**, 1588 (1987). doi:10.1126/science.3629258
33. J.M. Schierholz, J. Beuth, J. Hosp. Infect. **49**, 87 (2001). doi:10.1053/jhin.2001.1052

34. T. Haile, G. Nakhla, E. Allouche, Corros. Sci. **50**, 713 (2008). doi:10.1016/j.corsci.2007.08.012
35. S. Quintavalla, L. Vicini, Meat Sci. **62**, 373 (2002). doi:10.1016/S0309-1740(02)00121-3
36. H. Huang, Y. Yang, Compos. Sci. Technol. doi:10.1016/j.compscitech.2007.10.003
37. A. Top, S. Ülkü, Appl. Clay Sci. **27**, 13 (2004). doi:10.1016/j.clay.2003.12.002